
Article:
Mesaritis, M., Shamsa, M., Cuervo, P. et al. (4 more authors) (2020) A laboratory demonstration of rail grinding and analysis of running roughness and wear. Wear, 456-457. 203379. ISSN 0043-1648

https://doi.org/10.1016/j.wear.2020.203379

A LABORATORY DEMONSTRATION OF RAIL GRINDING AND ANALYSIS OF RUNNING ROUGHNESS AND WEAR

M. Mesaritis[1], M. Shamsa[1], P. Cuervo[2], J.F. Santa[2], A. Toro[2], M.B. Marshall[1], R. Lewis[1]

[1] Leonardo Centre for Tribology, Department of Mechanical Engineering, University of Sheffield, Sheffield, UK.

[2] Grupo de Tribología y Superficies, Universidad Nacional de Colombia, Medellín, Colombia.

Abstract
Rail grinding has been widely used for rail maintenance to keep the performance of the rail track at satisfactory levels. However, there is a lack of knowledge on the relationship between different grinding parameters and the effect on the rails and the post-grinding evolution of roughness and wear. Rail undergoes significant levels of stress during grinding to remove any defects that appear during its life-cycle which can cause significant microstructural change. By developing a method of demonstrating rail grinding it will allow further investigation of the process and potentially the exploration of different grinding patterns. Moreover, an analysis of the roughness of wheel and rail is an input parameter in most modern simulation tools that could be associated with the coefficient of friction. This paper reports a laboratory demonstration of rail grinding followed by a series of tests to determine the wear of the rail and if there is a relationship between friction coefficient and roughness. The rail specimens that were ground have undergone a phase transformation and showed White Etching Layer (WEL) on the contact surface. This was found to initially act protectively for the rail disc reducing the wear rates, but then contributed to crack formation. No clear long-term correlation was identified between the coefficient of friction and roughness during the testing, however a relationship could be drawn when test periods were studied individually.

Keyword: Martensite, White Etching Layer, Rail grinding, Railway maintenance, Derailments.

1 Introduction

Rail lines can sustain thousands of operating hours without replacement. However, in cities where rail transportation is one of the main methods of public transport the high usage of trains brings significant deterioration on the track structures due to rolling contact fatigue (RCF) and wear [1]. Therefore, a higher maintenance frequency is required in order to keep the rail lines in a safe and operational condition [2]. The wear on the rails might only be visible on the running surface, however corrugations and fatigue cracks will develop into internal defects as well. Rail grinding is used to minimize these external; and internal defects and reshape the rail line and maintain favourable rail profiles so that the operational life of the network is increased. The arrangement of stones on the grinding train over the rail varies at different angles. This arrangement is set to successfully reprofile the rail accordingly to achieve the maintenance requirements. A typical arrangement of the stones is presented in Figure 1-1.

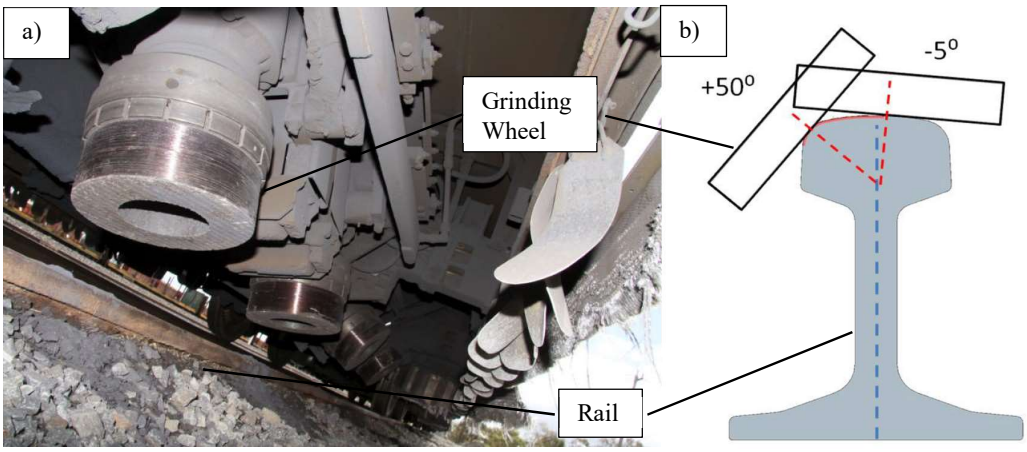

Figure 1-1: a) Grinding wheel arrangement on a train [3]**, b) Schematic showing the arragement of grinding stones for grinding of rails** [4]**.**

1.1 WEL

Although grinding is used as a maintenance process for re-profiling and removal of damage on rail lines (fatigue cracks, head checks etc.), in some cases this technique can significantly alter the mechanical properties of the surface and subsurface, affecting the overall performance of the rail [5]. The abrasive grains used, the applied pressure and speed between the train and the rails can be the deciding factors on the post-grinding material properties and topography. A problem occurring due to non-optimal grinding conditions being applied is the formation of White Etching Layer. This layer is essentially a thermally induced layer on the rail surface [6] created during high friction interaction between rail-wheel or rail-grinding stone.

The name White Etching Layer (WEL) is given by its high corrosion resistance to chemical etchings (usually with a mixture of 2-10 vol% of HNO_3 in ethanol) which makes it appear white under unpolarized light. WEL was observed for the first time by Stead on steel wire ropes [7]. Three main initiation mechanisms have been suggested for WEL: 1) extensive plastic deformation producing a single layer with really fine grains, 2) swift heating followed by swift cooling, 3) reaction of the material surface with the environment. Several studies have been made since then to clarify the mechanisms and their effect on the material performance and life cycle. However, it has been later concluded that two main mechanisms can be used to explain this phenomenon. The first one is based on the combined action of friction and heat, and the dislocation that occurs due to plastic deformation. The other mechanism occurs when temperature levels exceed the austenite phase transition temperature of the material combined with rapid cooling [7-8]. Generally, rails have a pearlitic structure with several microstructure variations accordingly to the manufacturer requirements. The structure remains stable up to 650°C. As temperature increases further the material transitions into the austenite phase. Any temperatures above this (around 700 °C) followed by rapid cooling will result in the formation of WEL or a martensite micro-layer on top of the surface.

1.2 Train derailment

Post-grinding rail roughness level has a big impact on the performance of the rails. For cases where roughness values were particularly low, flange-climbing derailments occurred [9][10], when a wheel of a rail vehicle climbs up a rail. The names used for relevant parts of wheels and rails and a typical sequence of events leading to a flange climbing derailment is shown in Figure 1-2. These are the most common causes of the derailments of trams [11], and of mainline trains [12] in the UK.

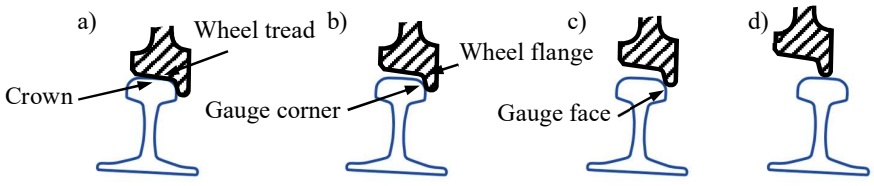

Figure 1-2: Typical development of a flange-climbing derailment: a) Initially, the wheel flange contacts the bottom of the rail's gauge corner, b) contact forces cause the wheel's flange to move up the gauge

corner, c) as the wheel moves higher up, a lower lateral force is needed to maintain movement, d) once the tip of the wheel flange is running on the crown of the rail, derailment is imminent if sufficient lateral force persists.

The simple force equilibrium was solved many years ago by Nadal [13]. Several analyses were done since then [14-16] with a focus on the force equilibrium concluding that if the lateral force or friction is high enough, or the vertical force or the contact angle small enough, the wheel will climb up the side of the rail. Thus, the most significant factor for flange-climbing is the friction associated with the wheel/rail contact. Similarly, it has been reported that the wheel/rail friction associated with freshly-ground rail can be high. Moreover, in rolling-sliding contact the ratio between the tangential and normal force (the coefficient of friction) depends on the amount of slip in the interface [16]. The largest value of this coefficient is comparable to the coefficient of friction and typically occurs for a slip of about 1% [17]. For higher slip the coefficient of friction typically reduces, probably because of the effect of frictional heating.

To enable an accurate simulation of a derailment, vehicle dynamics software uses friction between the wheel and rail as an input parameter (different values at the tread and flange are commonly analysed). Rail accident investigators would like to be able to estimate the appropriate value of friction using data measured at the scene of the derailment.

The aim of this study is to investigate the relationship between roughness and friction using twin-disc testing after grinding occurs and examine the consequences of having WEL on the specimens. The presence of a relationship between roughness and friction coefficient would facilitate simulations of accidents and will aid in avoiding them. This will be done by taking replicas of the wheel and rail's surfaces during the experiments and measuring their roughness afterwards (for details of a similar process see [18]). Further measurements would be done for the mass loss during the testing to identify how WEL affects the wear mechanism. Finally, the specimens will be sectioned after the testing to analyse their microstructure and investigate the effect of WEL on crack propagation and work hardening. The results would allow to investigate and understand the post-grinding performance of rails.

2 Literature Review

Both WEL and roughness are outputs of the grinding process, which can affect the performance of the rail differently. As mentioned previously, WEL can alter the life-cycle of the rail by introducing new defects and roughness can be interlinked with derailment incidents. This section will further investigate the research that took place on these two parameters.

2.1 WEL

Some representative studies from Rasmussen et al. [19] and Zapata et al. [20] investigated the formation of cracks due to the interaction between the rail material and WEL. Undeniably, it was found that cracks observed in their work were a direct consequence of the profile grinding. Consequently, WEL can reduce the resistance of the rail to rolling contact fatigue. Nevertheless, further study needs to be done for the clarification of the relationship between the thickness of the deformed layer and the grinding conditions.

In another study performed by Lin et al. [21] a specific inserted semi-artificial thermocouple method (ISTM) has been used to evaluate the effects of grinding pressure, rotational speeds and grinding stone size on grinding rail temperature. It was observed that the surface temperature increases significantly as the applied grinding pressure increases from 1000N to 2000N. Furthermore, surface temperatures above 600 ºC have been observed resulting in grinding burn situations which are accompanied by WEL formation. The peak surface temperature experienced was 802 ºC. At this point cracks formation starts to occur at the surface of the work piece. It was also concluded from the literature that two main mechanisms can be used to explain the formation of the WEL. The first one is based on the combined action of friction and heat and the increase of dislocations density that occurs due to plastic deformation [8]. The other mechanism is temperature levels above the austenite phase transition temperature of the material following with rapid cooling of the material [22]. An attempt was also made to create a relationship between the surface state, grinding burn and grinding temperature.

Full-scale testing was carried out by Uhlmann et al. [23] utilizing a face and profile grinding machine along with R260 rail specimens. The grinding was performed under laboratory conditions with a variation of wheel peripheral speed and depth of cut. It was determined that the surface roughness was directly affected by the peripheral speed of the grinding wheel. In addition, different hardness profiles were observed on the surface layer caused by different peripheral speeds and cutting depths. Elevated peripheral speeds of the grinding wheel and higher cutting

depths have led into increased hardness Moreover a correlation between the Barkhausen noise and the specific grinding energy that was used.

Although the abovementioned studies successfully generated a WEL due to a grinding process, it is uncertain whether the methodology used effectively simulates the conditions exist in the field. The experiments presented in this study can overcome these doubts by using equivalent parameters used in field (forward speed and grinding stone speed) and identical materials (grinding stone and rail specimens).

2.2 Post-grinding roughness

There have been a number of studies on the effect of surface roughness on coefficient of friction. The previous twin-disc tests are summarised in Table 1. They all compared the coefficients of friction at specific numbers of cycles (between 500 and about 16,000) after the roughness had been measured. They showed that initially rough wheels are associated with lower coefficients of friction, and Table 1 indicates for which range of cycles their results were valid. No study has tried to find out if and how the coefficient of friction varied as a function of the roughness.

Table 1: Twin-disc studies on the effect of roughness on coefficient of friction, all showing that initially rough wheels are associated with lower coefficients of friction.

Reference	Wheel roughness (μm)	Rail roughness (μm)	Slip (%)	Contact pressure (GPa)	Cycles at which coeffs of friction were compared	Notes
Fukagai et al. [24]	0.2, 3.5, 6.2 (Ra)	1.1 (Ra)	2 + 1° AOA**	2.2	Up to 500	Tapered surfaces
Doi et al. [25]	0.17, 18.9 (Ra)	0.60 (Ra)	0.3	0.56*	Not specified (16,000*)	
Lundmark et al. [26]	2, 14 (Sa) 2 (Sa) 14 (Sa)	0.5 (Sa) 2 (Sa) 0.5, 2 (Sa)	1	0.81 – 0.88	At 10,000 – trends unclear in first 2000 cycles	Lower μ for smoother rail

* Calculated using data from [27]
** Angle of attack

Lundmark et al. [26], as well as studying different wheel roughnesses, included different rail roughnesses by grinding perpendicular to the direction of rotation. They found that rougher rails were associated with higher coefficients of friction. However, during the first few thousand cycles, their rankings were not clear. They found the same rankings at 10,000 cycles for 4 different combinations of wheel and rail materials.

Full-scale tests [18] found that smooth wheel on rough rail (case 1) was associated with a lower coefficient of friction than rough wheel on smooth rail (case 2). Tests were carried out at 3% slip with a Hertzian stress calculated to be about 1.3 GPa. The tangential roughness (Rq) of wheel and rail were 6.9 and 1.2 μm for case 1, and 0.8 and 2.4 μm for case 2. From this study, the coefficient of friction associated with case 1 was found to be about 0.21, and for case 2, about 0.26. Using data from the end of the tests, more coefficient of friction and roughness values were presented: for tangential wheel/rail Rq of 3.5/2.3 μm, the coefficient in case 1 was about 0.48; while for case 2, 1.1/2.0 μm corresponded to a coefficient of friction of 0.5.

In summary, this study will attempt to simulate the conditions and the mechanisms of the grinding process that occurs in the field by utilizing an actual grinding stone and R260 rail specimens that were directly machined from a rail. Also, the performance of the ground specimens will be studied post-grinding to analyse the coefficient of friction and roughness development during the initial run-in period. This will reveal any correlation that might exist between the roughness and coefficient of friction.

3 Specimens and Methodology

The experiments were done with the purpose of simulating the maintenance procedure that takes place in the field. Thus, grinding was performed on rail specimens and after that, using a test-rig that simulates the rolling/sliding mechanism, the run-in behaviour of the specimens was recorded. Moreover, the post-grinding performance of the specimens was studied with the purpose of understanding the roughness development to correlate it with

potential derailment issues. Finally, considerable attention was given to the WEL and how this might affect the initiation of rail cracks.

3.1 Materials

The rail specimens used were machined from a rail section of grade 260. The rail was machined to give a disc with contact width of 10 mm and a diameter of 47 mm. The wheel was machined from a BS5892-3 grade R8 wheel. Composition of rail and wheel material is presented in Table 2 along with mechanical properties.

Table 2: Chemical composition (wt%) and mechanical properties of rail and wheel samples [28][29]**.**

	C	Si	Mn	P	S	Cr	Al	V	Cu	Ti	Ni	Mo
R260	0.736	0.270	1.056	0.032	0.023	0.026	-	0.003	0.002	0.016	0.021	0.006
E8	0.542	0.253	0.734	0.011	0.06	0.141	0.027	0.006	0.165	0.002	0.120	0.048

Tensile Strength (MPa)	
R260	≥880
E8	860-980

3.2 Rail grinding testing

The equipment used for the grinding is presented in Figure 3-1. The grinding wheel is coupled to a motor that runs at a fixed speed. The whole grinding wheel-motor structure is placed on roller bearings to allow linear movement towards the rail disc and perform grinding. The grinding wheel was acquired directly from the field and has identical specifications to the ones used in rail grinding. It is resin bonded Al_2O_3 and the dimensions comply with the US standards. The test rig was designed and manufactured by the Grupo de Tribología y Superficies at the Universidad Nacional de Colombia.

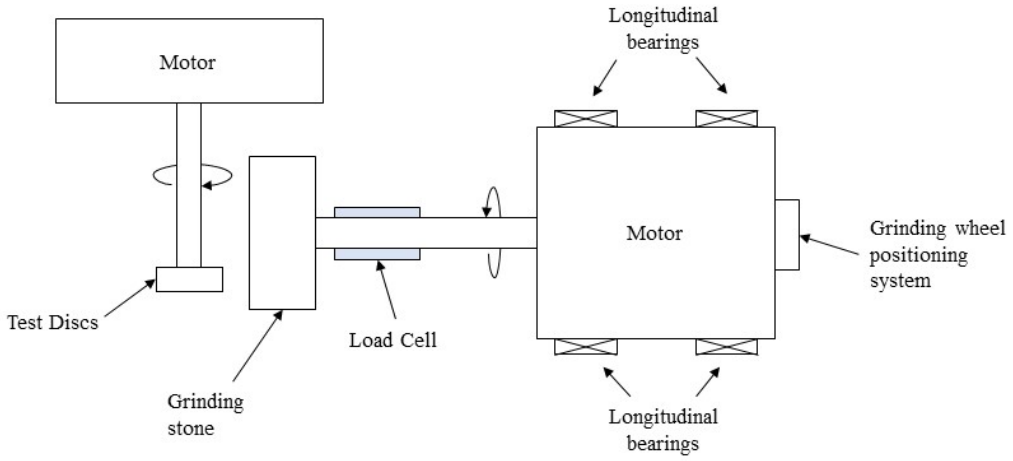

Figure 3-1: Schematic representation of the equipment used in the grinding experiments.

As soon as the grinding wheel and rail discs reach their required speed, the grinding wheel is moved towards the rail specimen. The grinding time starts when the first sparks appeared. After the first contact for this study a load of 5kg was maintained during the testing for 30 seconds. Then the experiment was terminated. The testing parameters utilised during the experiments are presented in Table 3. The rail specimens were then removed for measurements to be taken on the material removed in terms of mass and diameter. This procedure indicated the completion of one pass. Multiple passes were done to reach a 0.25mm depth of cut on the radius of the disc.

Table 3: Testing parameters for multiple passes experiments.

Grinding Wheel Speed (Vs -rpm)	Specimen Speed (Vw - rpm)	Applied Load per pass (N)	Depth of Cut (mm)	Overall Grinding Time per pass(s)

3600	700	49.05	0.25	30

3.3 Twin disc testing

A rolling contact test was carried out to generate wear and cracks on the discs simulating the possible damage of rails in the field. For this experiment, SUROS, an already existing test rig was used to simulate the rolling/sliding movement between rail and wheel. This method has been used in other studies as well [30][31]. The test rig uses discs that were extracted from rails and wheels, with similar geometry to the specimens described in section 3.1 The results shown in this work describe the average behaviour recorded. During the testing the torque between discs was measured and used to calculate the tangential force. The tangential forces were then used to determine the coefficient of friction for the contact. The length of the contact zone is the transverse width of the cylindrical sample (10mm).

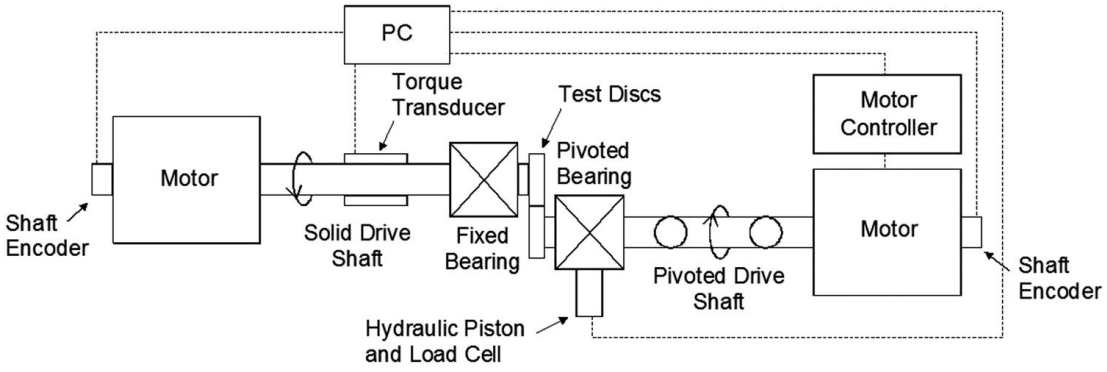

Figure 3-2: Schematic of the SUROS machine.

To assess whether the friction associated with a particular wheel/rail roughness could be determined, a twin-disc test was undertaken. The test was performed under 1% slip and a contact pressure of 1.3 GPa. The rail disc used was previously ground whereas the wheel disc had a freshly machined surface to represent freshly-ground wheel/rail interface. However, the grinding marks were around the disc; orthogonal to that expected in the field. The coefficients of friction were monitored in the test, and the surface roughness was determined at intervals during the test by using the procedure described in [18]. For the first 600 cycles surface roughness data were taken every 200 cycles and then measurements were taken every 400 cycles for up to 3800 cycles. Then the test was run with no interruption until 8000 cycles. The procedure followed for the surface roughness measurements is described below:

- Stopping the test and waiting for the discs to cool
- Cleaning the discs in an acetone bath
- Applying a layer of Microset 101 Thixotropic replicating compound to the disc's surfaces, adding a piece of backing paper, and waiting six minutes for the replica to set
- Using an Alicona InfinateFocusSL 3D measurement system with a 5X magnification lens and a cut-off wavelength of 800 µm to create a digital representation of the surface of the replica
- Choosing lines with a minimum length of 4 mm on the digital image along which the Alicona software calculated roughness measures
- Cleaning the discs in an acetone bath
- Mounting the discs to continue the experiment

Throughout the test, the laboratory temperature was 25°C, and humidity varied between 26% and 31%.

3.4 Analysis of ground disc's metallography

To analyse the microstructure of the tested discs, the specimens were sectioned to acquire a cross section and longitudinal view. Figure 3-3 represents how sectioning occurred and the viewing plane that was analysed.

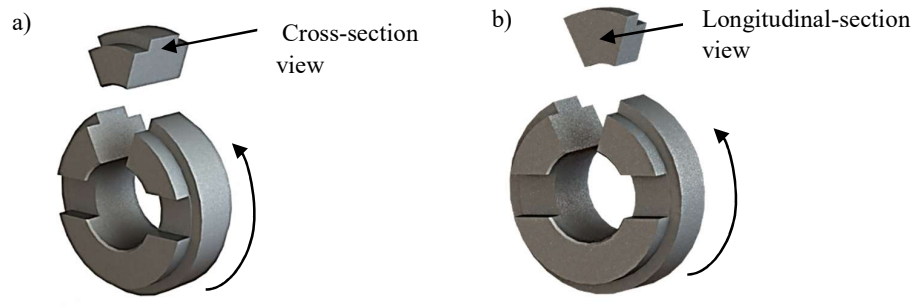

Figure 3-3: Representation of the material sectioned from the discs a) a cross-section of the disc specimens b) longitudinal-section of the disc specimens.

After the test, discs were sectioned, they were polished and etched in 2% Nital to allow examination of the microstructure and the cracks. using both optical and scanning electron microscopy.

4 Results

The data obtained from the test and sectioning are presented in the following sections.

4.1 Microstructure Analysis

Figure 4-1 shows the microstructural analysis of the rail discs straight after the grinding testing had taken place. Several microscopic images were taken of the ground discs to identify the effect of grinding on a microstructure level. As it can be clearly seen in Figure 4-1, White Etching Layer (WEL) exists in all orientations of the discs' microstructure. The WEL occurred on top of the contact surface, which indicates material transformation during the grinding process. A maximum thickness of 5.75µm was detected in the disc cross-sectional view.

Specimens from the field have been acquired right after grinding took place for comparison between laboratory and field. The samples were polished and etched following the same procedure with laboratory specimens. The grinding parameters used on the field were similar to the parameters used during the laboratory experiments with a maximum depth of cut to be 0.5mm. A phase transformation also exists on the top of contact surface with a maximum thickness to be around 11µm. It is worth mentioning that the sample acquired was from the gauge corner of the rail. Similar WEL thicknesses were identified on field sample after grinding by Rasmussen et al. [19].

As mentioned previously the two main mechanisms identified to explain the WEL formation are: 1) the combined action of friction and heat and the dislocation that occurs due to plastic deformation; 2) the effect when temperature levels increase above the austenite phase transition temperature of the material and are followed by the rapid cooling of the material. In the current experiment the mechanism that would be most appropriate to explain the transformation is high stresses and high temperature produced in the contact zone due to the combined action of friction and heat and material dislocation that occurs due to plastic deformation during grinding.

	Cross sectional view	Longitudinal-section view
Microscope image 1	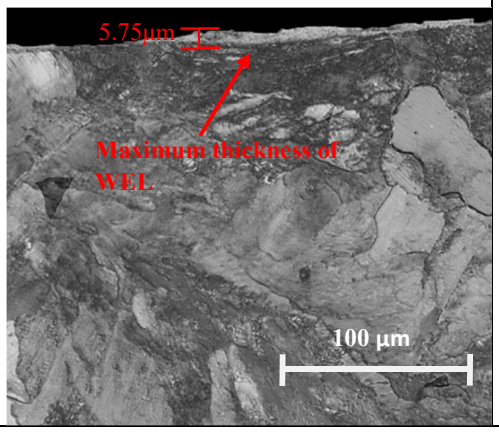	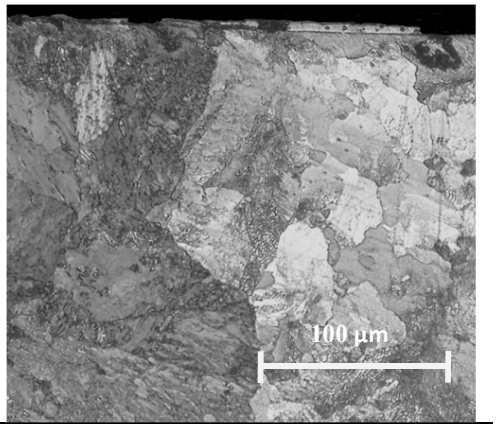

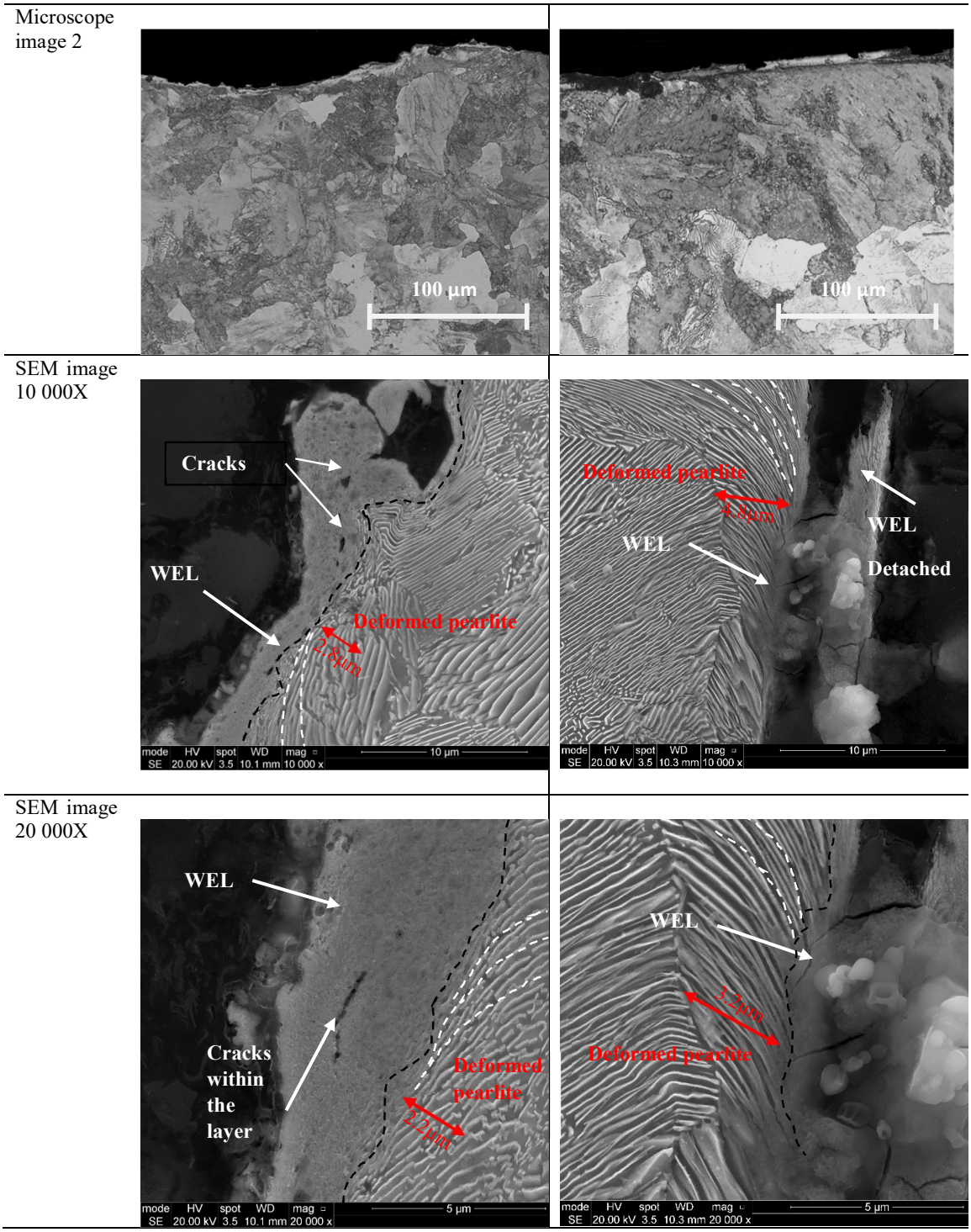

Figure 4-1: Optical and SEM images of the rail specimen microstructure post grinding.

The plastic deformation after the grinding process is clearly visible in Figure 4-1. SEM images at 20000x magnitude exhibit the deformed ferrite and cementite layers near the transformed WEL area. In the longitudinal section the deformed layer is significantly larger than the equivalent cross-sectional view ranging between 4.8-3.2µm compared to 2.8-2.2µm in the cross-sectional view. A study by Zhou et al. [32] also supports that there is

plastically deformed layer between the WEL and the bulk material, however, the magnification used in that study was not adequate to distinguish this.

In Figure 4-2, images from a ground field samples of an R260 rail are presented. The depth of the WEL in samples ground in the field (around 6µm) is comparable to the thickness found for samples ground in the laboratory. Additionally, the same values have been reported in the literature by by Rasmussen et al. [19] on a same material grade field sample. The SEM image also exhibits the presence of a deformed layer near the WEL. However, it should be noted that the field samples have undergone some usage previously which might have contributed to the formation of the deformed layer.

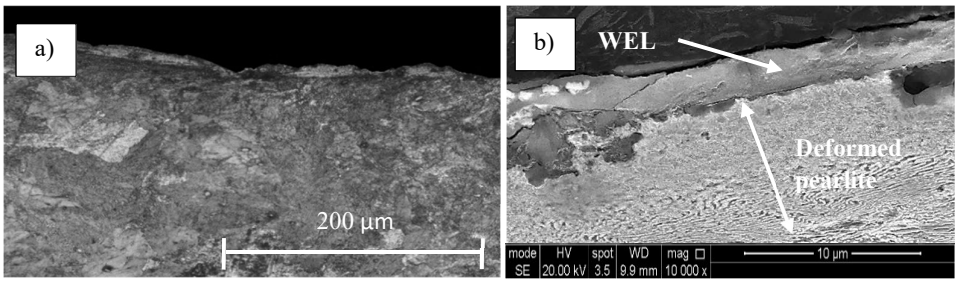

Figure 4-2:Microstructure images from an R260 field samples by a) Optical microscope b) SEM

In Figure 4-3 the microstructural analysis of the discs after the twin-disc testing is presented. The images obtained were from an Optical Microscope and SEM.

	Cross sectional direction	Longitudinal section view
Optical microscope image 1	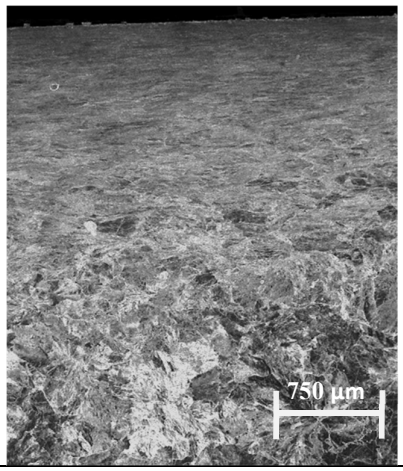	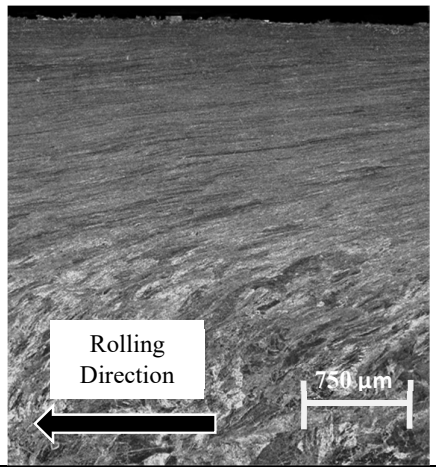
Optical microscope image 2	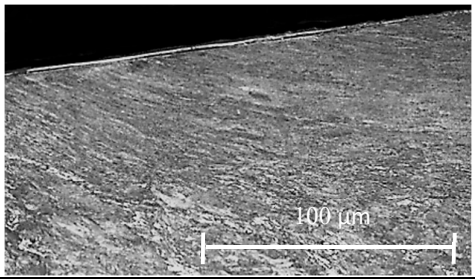	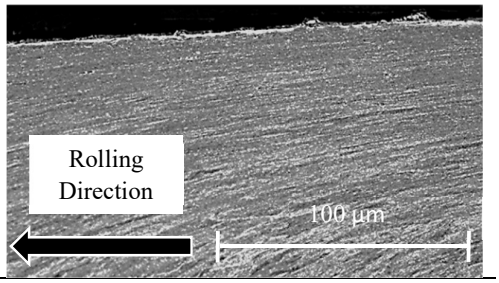
SEM image 10 000x		

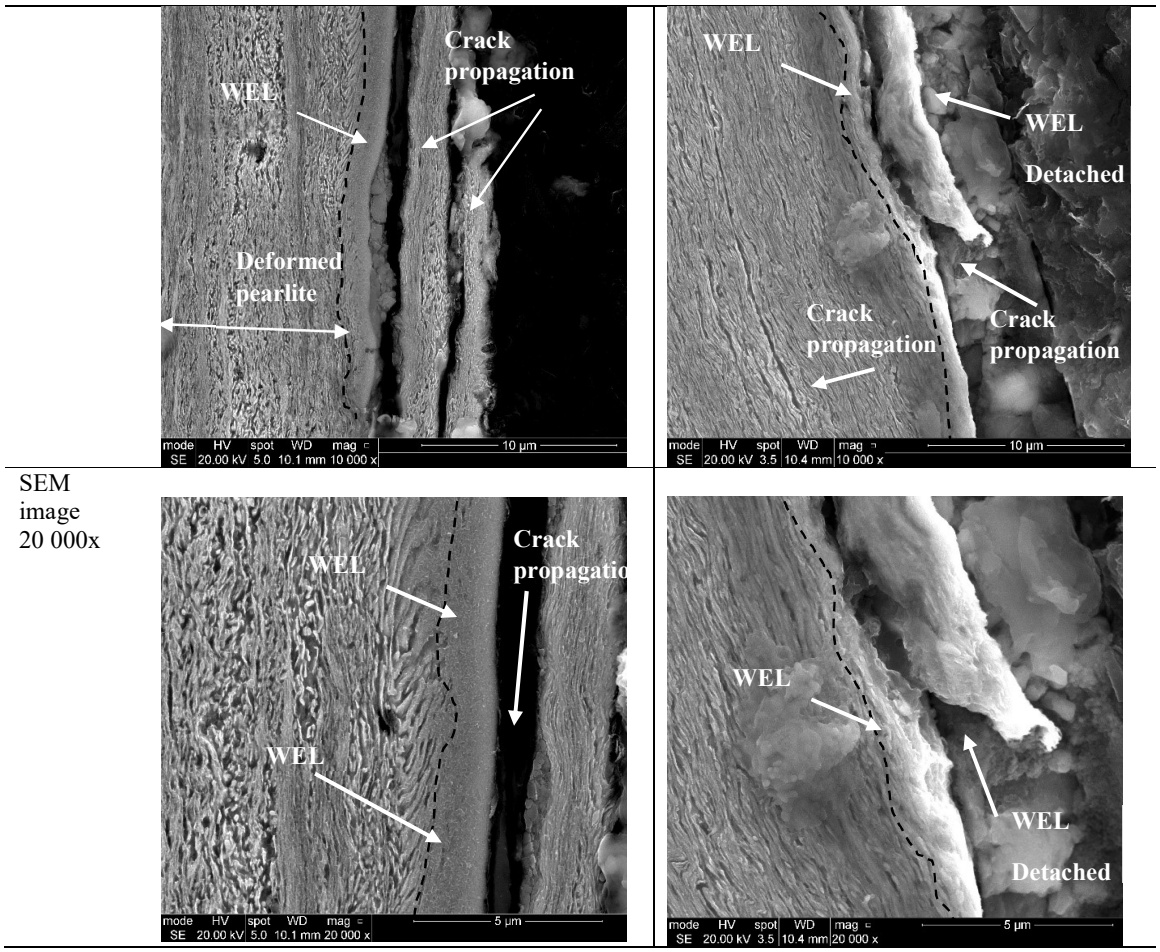

Figure 4-3: Optical and SEM images of the rail specimen microstructure after the post-grinding rolling/sliding testing.

After the rolling contact testing on the ground disc the WEL has become encapsulated below the bulk material as it can be seen in Figure 4-3. The significant difference of the properties between the WEL and the pearlitic microstructure could be the factor cracks initiated during rolling contact experiments.

Further images were taken on SEM under high magnification to clearly identify how WEL affects the crack propagation on the rolling contact experiments. The images in Figure 4-4 present clear examples where WEL is

trampled between pearlite. This resulted in cracks being initiated and propagating more easily near where WEL was presented.

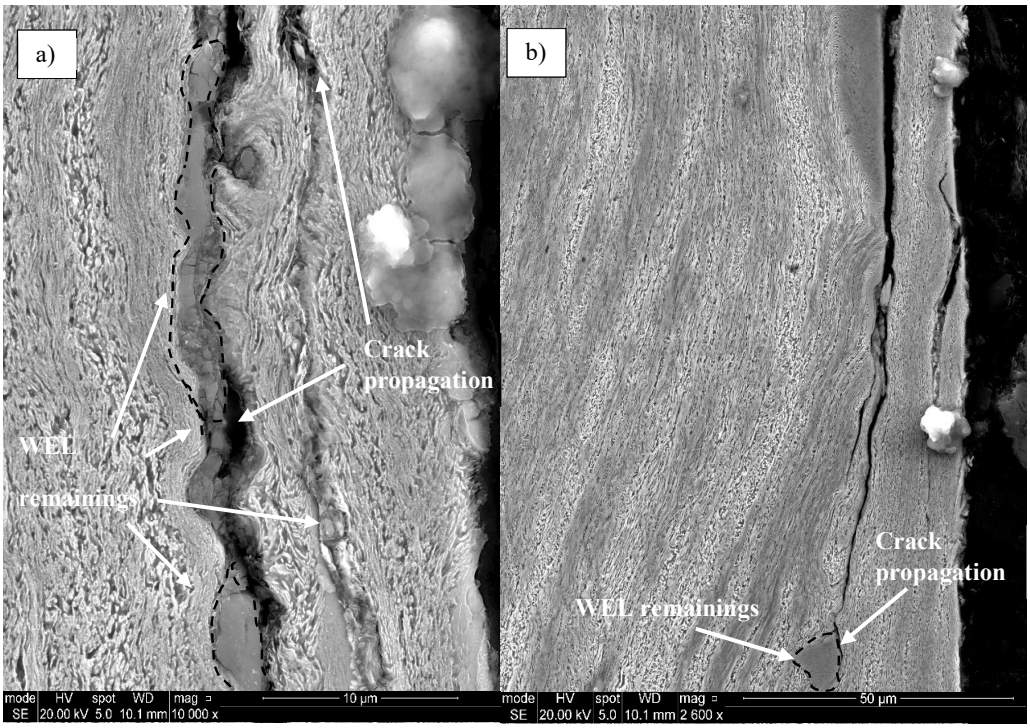

Figure 4-4: SEM images representing the initiation of cracks at the points were WEL remainings were squashed around pearlite.

The schematics in Figure 4-5 aims to imitate how the surface roughness develops during the rolling contact testing. During the first few hundred cycles the asperities are smoothed out and the WEL starts to crack due to its high brittle nature. As a result of the shear forces, during the testing, pearlite starts to deform slightly in the opposite direction of the rolling contact testing resulting in the slight overlay of the WEL. Finally, after a couple of thousand cycles the WEL was crushed into smaller pieces. Some of the pieces detached from the disc and the ones with a stronger bond remained attached. The pearlite undertook significant plastic deformation up to this point. However due to the fact that WEL cannot be plastically deformed, it is acting as obstacle during the deformation of pearlite. Thus, the remaining WEL is squashed by the pearlite as presented in Figure 4-3 and Figure 4-4. Finally, this results in cracks being initiated where the WEL remainings exist as clearly observed in Figure 4-4.

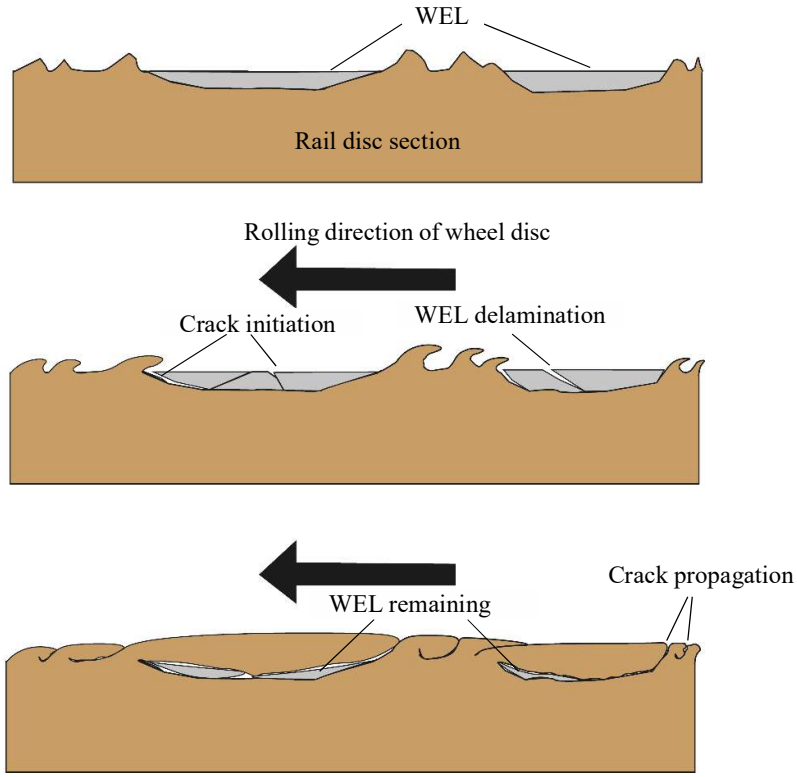

Figure 4-5: Schematic explaining the run-in mechanism during the post-grinding rolling contact experiments.

4.2 Hardness of disc specimens

The hardness of the disc was measured in two instances, after the grinding experiments and following the twin-disc testing of 8000 cycles under 1% slip to perform a comparison between the hardness of the material. The micro-hardness testing took place with a load of 0.3kg in multiple locations starting close to the outer rim of the disc and moving towards the centre of the section to observe any work hardening effect occurring near the running surface of the disc. Images from the surface were also taken (Figure 4-6 & Figure 4-10). A micro-hardness test was also performed on the WEL just after grinding to clarify the martensitic properties. The load used was 0.1kg since the indentation area had to be reduced to be accommodate within the thickness of the WEL.

Starting at a distance of 0.1mm from the surface of the disc the hardness of R260 right after the grinding testing was averaged at 285Hv indicating that there was not any hardening of the material during the grinding process on that scale. The indentations performed on the specimen and the depths of them are presented in Figure 4-6. These results do not necessarily mean that the material was resisting plastic deformation. The consequences of plastic deformation occurred in the material might be presented in the form of WEL since one of the main causes of WEL formation is the excessive plastic deformation. Nevertheless, in Figure 4-1 where the microstructure of the specimen is observed on a microscale level, a thin deformed layer of 4μm was identified near the WEL. This thin layer was not detectable by the normal hardness testing that took place. The thin deformed layer indicates that the grinding process efficiently removed material without losing a lot of energy on plastic deformation. Also, energy losses must have occurred due to heat dissipation into the bulk material.

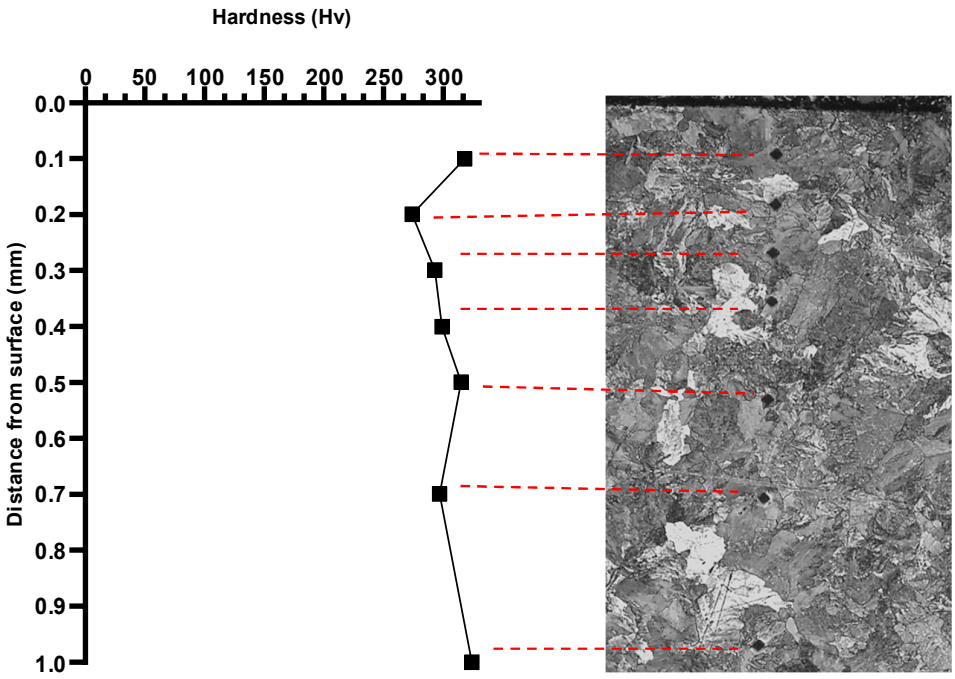

Figure 4-6: Hardness testing on the specimen after grinding testing at a depth of 1mm.

As mentioned above, the hardness of the top layer where the phase transition occurred was measured to clarify the existence of a martensite layer as it can be seen in Figure 4-7. A hardness of 1093Hv was measured which indicates, the layer is significantly harder than the bulk material. Moreover, this suggests the WEL would be more brittle than pearlite. A brittle layer could affect the life of the material since cracks can be more prone to be initiated due to the brittle nature of the top layer. Similar observations on WEL hardness were made by Zhou et al. [32] and Rasmussen et al. [19].

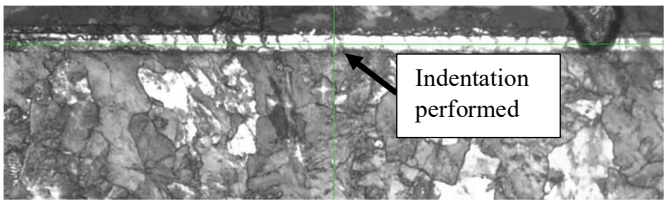

Figure 4-7: The indentation on the WEL(cross showing the position of the indentation.

Since the micro-hardness testing allowed very limited number of indentations on the WEL, further nano-hardness testing was performed with indentations up to 20µm below the running surface of the sample and 2µm distance between indentations to clarify the existence of WEL and obtained a better resolution of the hardness fluctuation. The nano-indentations allowed to obtain the nano-hardness and elastic modulus of WEL and bulk material along the depth of the specimen clarifying the existence of a harder more brittle layer. In nano-indentation testing, the load-displacement data are obtained allowing the calculation of mechanical properties and elastic-plastic behaviour. Hysitron TI Premier was used with a Berkovich intender using 2000µN force. Data obtained are presented in Figure 4-8 with the load-displacement curves and Hardness-Reduced Young's modulus data. The WEL hardness was determine between 1089-779Hv with the bulk material hardness averaging at 228Hv. Between these two areas a transition region from the WEL to the bulk material was identified with hardness values between 779-375Hv.

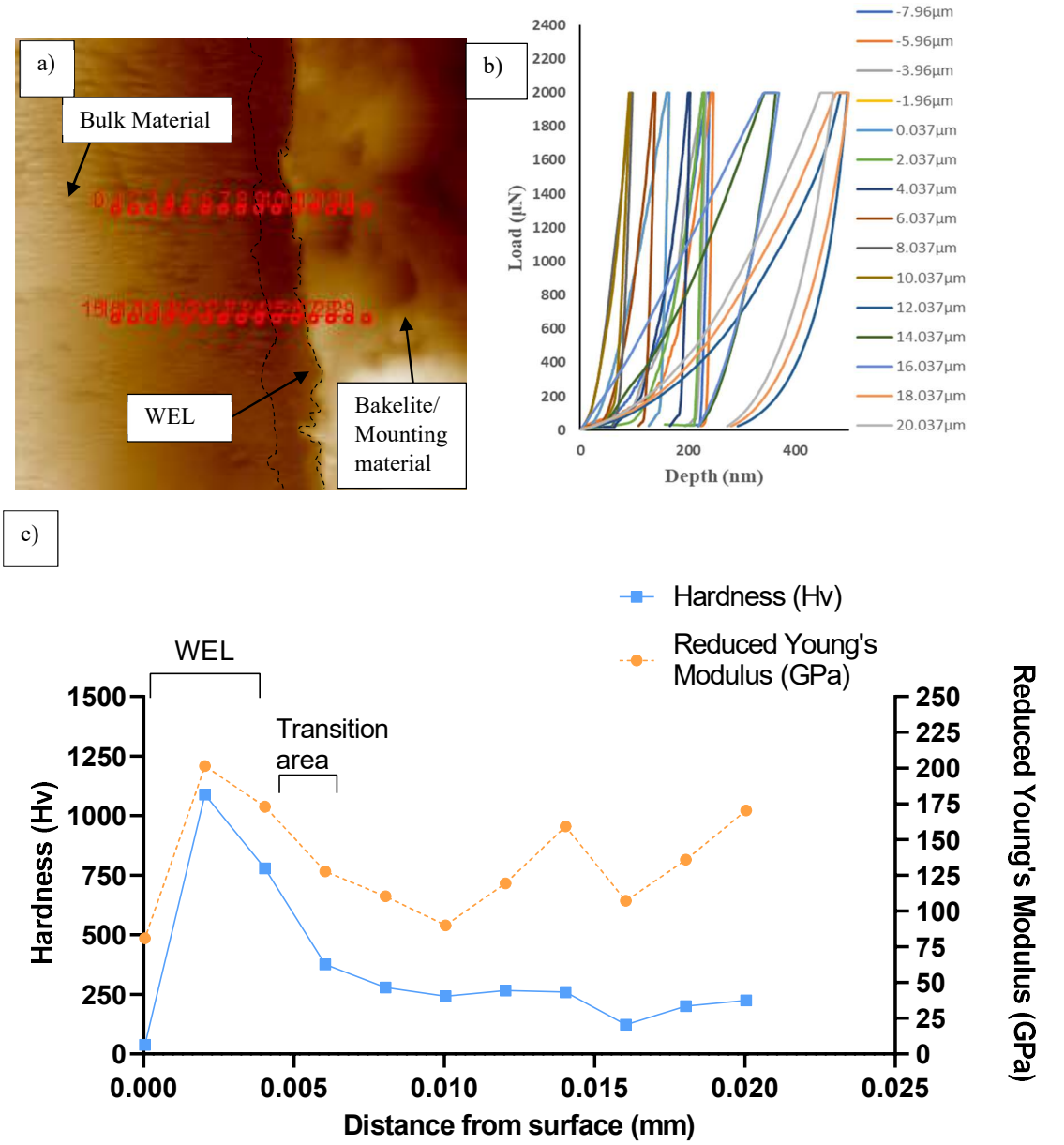

Figure 4-8: Indentations performed on the WEL and bulk material of the R260 laboratory specimen; a) Scanning probe microscopy (SPM) on the area the nano-indentations will be performed with the indentations; b) Load-Displacements curves from the experiment; c) Nano-hardness and Reduced Young's modulus along.

Additional testing was done on a sample obtained from the field to acquire the nano-hardness and elastic modulus of a ground field sample from the same rail material. This will allow further comparison of the mechanical properties of WEL formatted on the laboratory sample and on the field sample. Data obtained are presented in Figure 4-9. The nano-hardness of field sample was determined at a range between 1500 – 1074Hv for the WEL area. A transition area was also identified between the WEL and bulk material with hardness ranging between 649 - 410Hv. The nano-hardness of bulk material was determined at a mean value of 328.1Hv. The hardness values of the field sample are slightly elevated compared to the values of the laboratory sample. However, in both cases the WEL hardness was significantly higher than the bulk material fluctuating around 1000Hv. Considering both datasets obtained from the laboratory and the field, the capability of the laboratory test rig to produce comparable results can be distinguished.

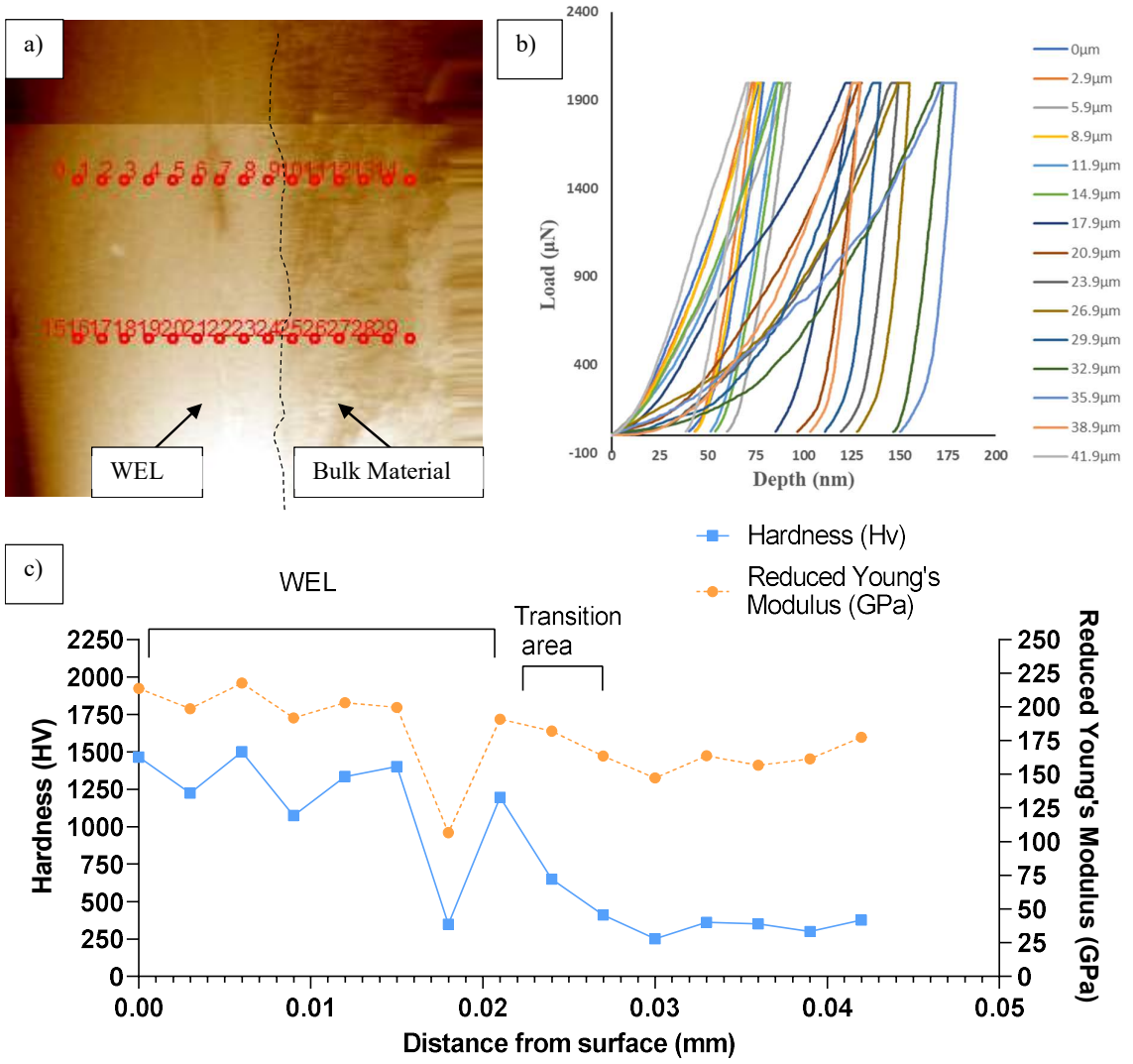

Figure 4-9: Indentations performed on the WEL and bulk material of the field specimen; a) Scanning probe microscopy (SPM) on the area the nano-indentations will be performed with the indentations b) Load-Displacements curves from the experiment, c) Nano-hardness and Reduce Young's modulus.

Figure 4-10 represents the hardness profile of the R260 right after the twin disc testing. A linear trajectory towards the centre of the disc up to 1.0mm below the surface of the material was done with 6 indentations. As it can be seen the material has undergone a hardening process during the twin-disc testing increasing the hardness up to a value of 500Hv. The fluctuation of hardness extends to a depth of 0.7mm below the surface of the disc. This indicates a change of approximately 200Hv compared to the bulk hardness determined in Figure 4-6.

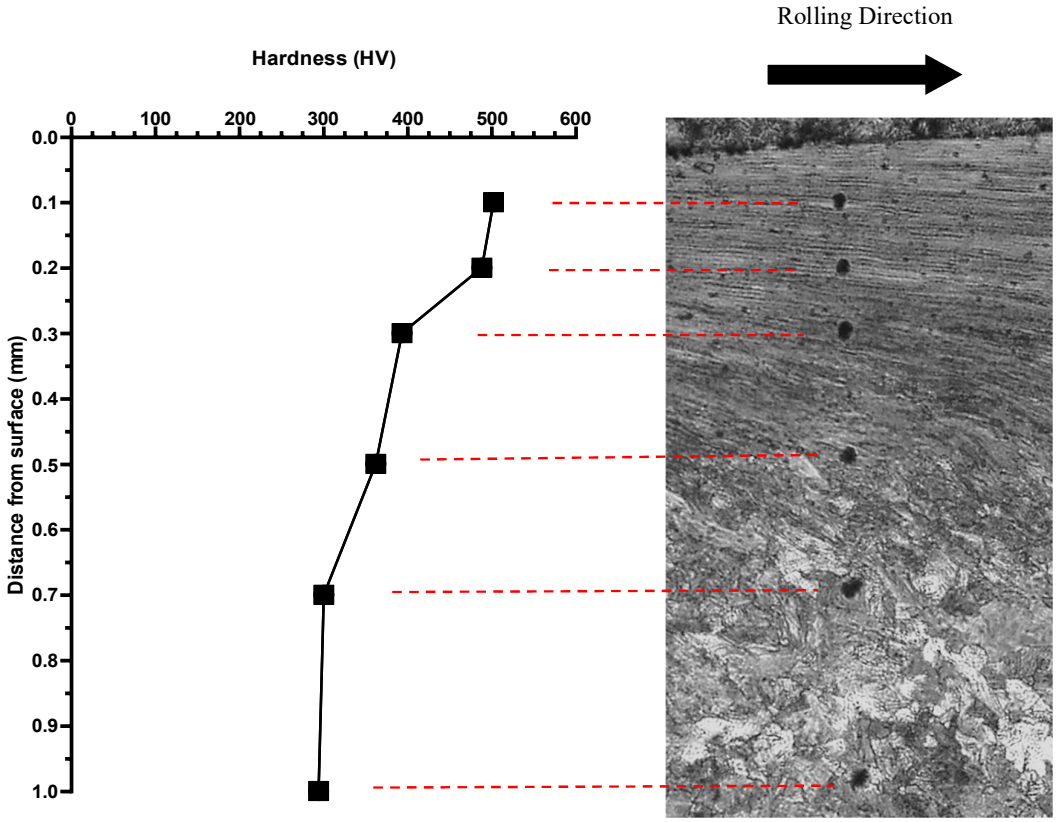

Figure 4-10: Hardness testing on the specimen after twin-disc testing up to a depth of 1mm.

4.3 Twin disc friction and roughness data

The measured coefficient of friction and slip provided by the SUROS machine during the test (1% slip) are shown in Figure 4-11.

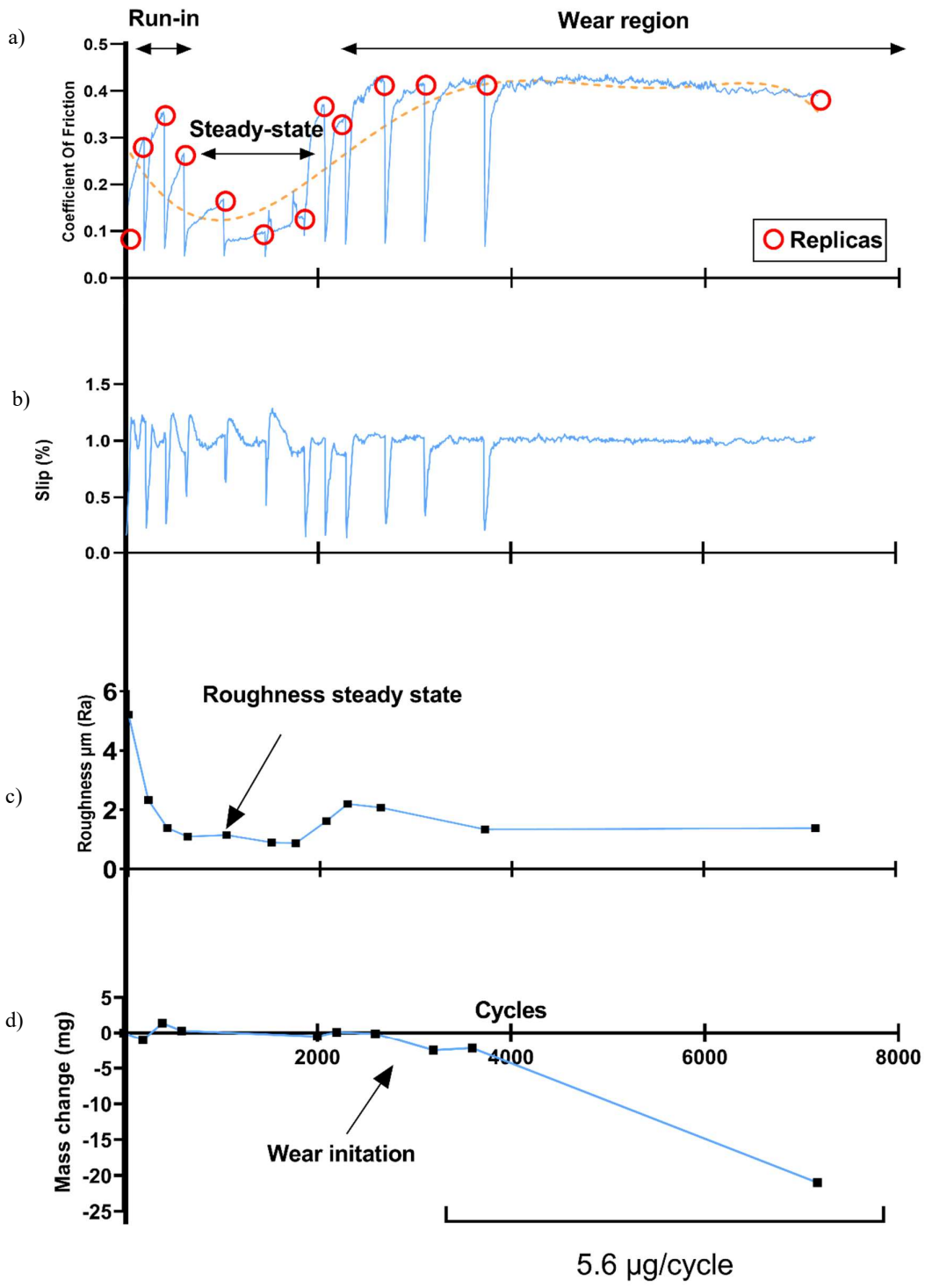

Figure 4-11: Data recorded from post-grinding twin disc experiment: a) Coefficient of friction; b) Slip; c) Roughness (Ra); d) Mass change.

As it can be seen in Figure 4-11 small cycle intervals were performed up to 3800 cycles where friction coefficient was stabilised and then the test was run up to 8000 cycles with no further stops. The rough surface of the rail at the start of the test resulted in high friction coefficient between the two bodies. Following the smoothing of the asperities and reduction of the roughness the coefficient of friction also followed a reduction. Finally, when the roughness rises again due to wear the friction coefficient rises as well. Hence, an initial correlation between the roughness of the rail surface and the friction coefficient was observed.

Data were also collected regarding the mass loss of the rail discs. Apart from the minor increase at 400 cycles (see Figure 4-11d) two main regions exist in the wear behaviour. From the starting point up to 2000 cycles there was no significant mass loss. In fact, during this period the discs seem to have collected some mass from the wheel disc that it was interacting with. The rail disc enters a wear region after 2600 cycles with significant losses occurring at a rate of 5.6μg/cycle, reaching the maximum amount of 25.5μg. The total wear rate of the test was determined at 3.57 μg/cycle. This behaviour is in agreement with the previously mentioned statements of the wear region that occurs slightly after 2000 cycles resulting in an increase of the friction coefficient.

To visualise any relationship between roughness and coefficient of friction, plots showing how the two parameters varied were prepared. These are shown in Figure 4-12. The error bars on coefficient of friction considered the values recorded for approximately the previous 50 cycles (first 50 for first value). Note that since there is no slip in the lateral direction, only the longitudinal roughness is considered.

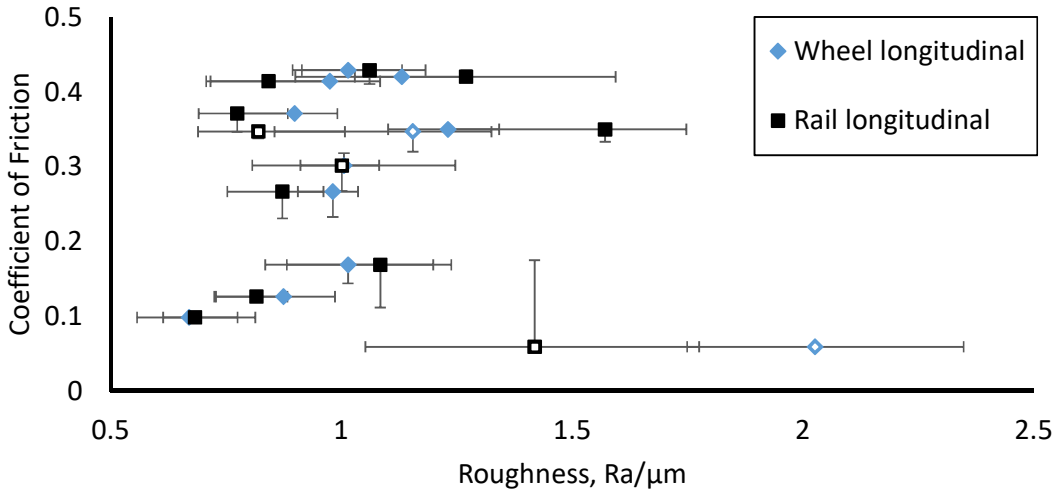

Figure 4-12: Development of wheel and rail roughness during rolling contact test (1% slip).

The data presented in Figure 4-12 do not demonstrate a trend between the coefficient of friction and roughness in either case (wheel or rail). This occurs due to the data in the graph cover three different regions run-in, steady-state and wear region. By separating the regions into three individual plots as presented in Figure 4-13 a trend can be clearly observed between coefficient of friction and roughness.

Figure 4-13a) which is the run-in region, exhibits clearly that as the roughness of rail increases, the coefficient of friction decreases significantly. This can be associated to a study by Fukagai et al. [24] where rougher machined wheel surfaces contribute to a lower coefficient of friction. With regards to Figure 4-13b) which shows the steady-state region, datapoints are situated randomly and do not form a relationship between the coefficient of friction and roughness. Furthermore, for Figure 4-13c) which demonstrates data of the wear region, it can be observed that coefficient of friction lies within a short range (0.35-0.42). Although a rough linear relationship between the parameters can be observed, it is still ambiguous due to fluctuation of the coefficient of friction, thus a clear conclusion could not be made.

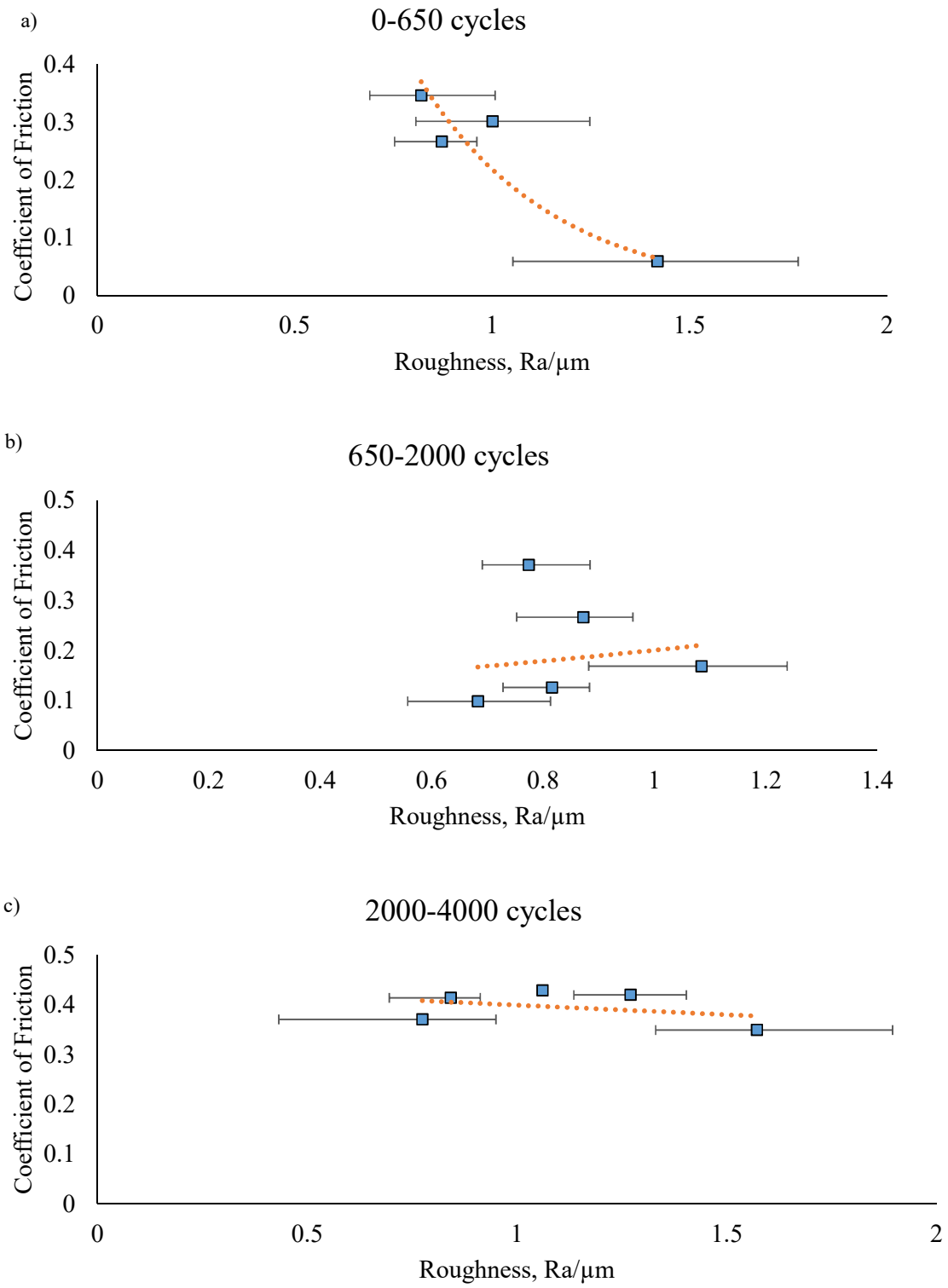

Figure 4-13: Roughness data against the coefficient of friction for rail disc during the experiments split into three plots: a) run-in; b) steady-state; c) wear region.

Figure 4-14 shows the profiles of the disc on 4 points, at 0 cycles, 1800 cycles, 3600 cycles and 8000 cycles. The analysis of the profile was done on a Bruker Alicona machine that utilises a focus-variation optical system. From

the scans the topographical information of the specimens was acquired in digital form for further analysis. The profiles exhibit the transition of the rough profile of the ground disc to a smooth profile after the initial run-in and then the increase of roughness due to the development of cracks.

Cycle	Picture	3D Image/Profile	
0	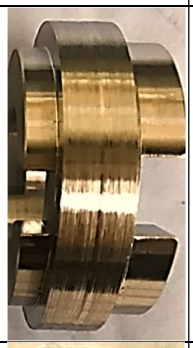		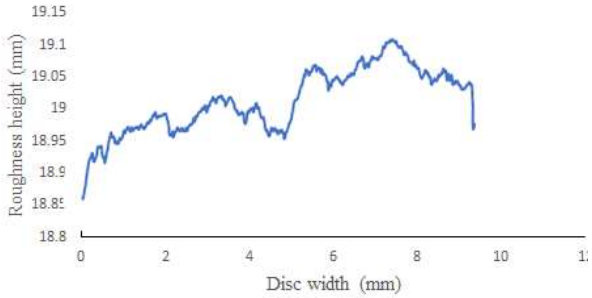
1800	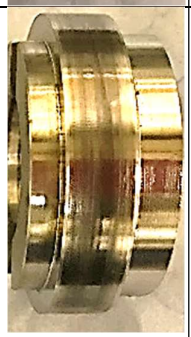	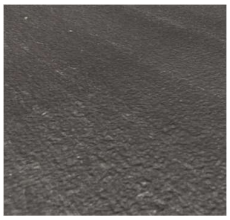	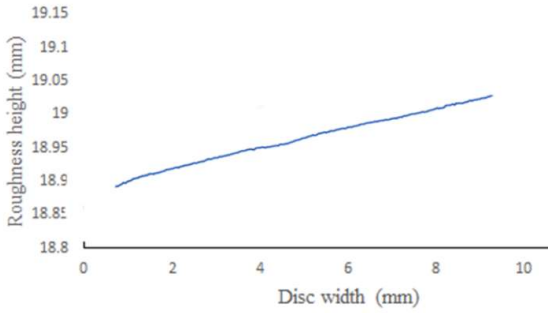
3600	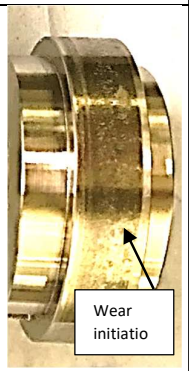	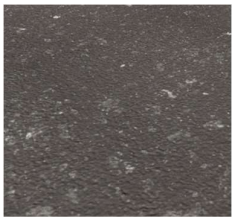	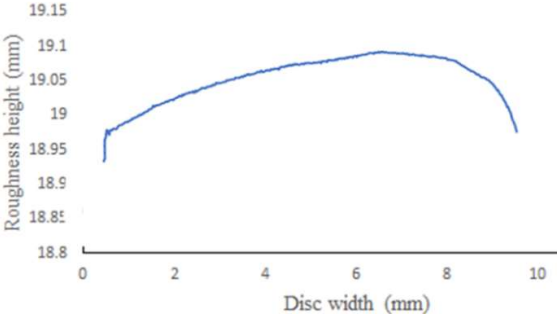
8000	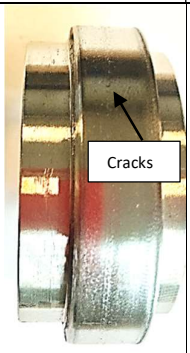	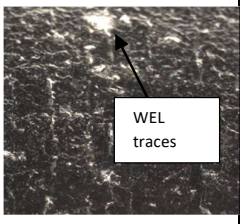	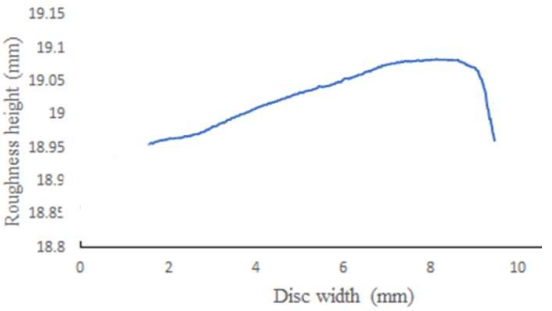

Figure 4-14: Surface of discs throughout the testing.

5 Discussion

The R260 rail disc underwent a multiple pass grinding experiment. This exhibited a WEL of approximately 6μm thickness after 0.25mm of material was removed from the radius of the disc. This material transformation could have been caused by the excessive material that was removed on each single grinding pass. Moreover, the multiple pass experiment possibly allowed the discs to cool down in-between passes. As a result, a benchmark comparison with the performance of a single pass grinding experiment should take place on discs, removing the same amount of material, to identify whether the continuous interaction with the grinding stone would produce thicker WEL on the contact zone.

As for the effect of WEL on the life-cycle of the rail discs, previous studies suggested [33][34]that the martensite layer on top of the rail can cause crack formation at a later stage. Other studies [35]concluded that the martensite layer delaminates with consecutive train operation. However, the induced martensite at the groove edges can cause excessive crack initiation on the rail line and reduce the normal RCF rail life by a factor of nine. As it can be seen in Figure 4-3 and Figure 4-4 from the SEM images, cracks can be initiated by the brittle nature of the WEL and propagate to the bulk material. However, as clearly represented in Figure 5-1 a comparison between the cracks generated on the same material disc that did not go through a grinding experiment and underwent 8000 cycles with 1% slip the number of the cracks do not have any significant differences. Nevertheless, the length of the cracks is larger on the WEL sample measured at 487μm compared to 178μm in the no-WEL sample. Further testing needs to take place to clearly identify that WEL affects the length of the cracks initiated during an RCF testing.

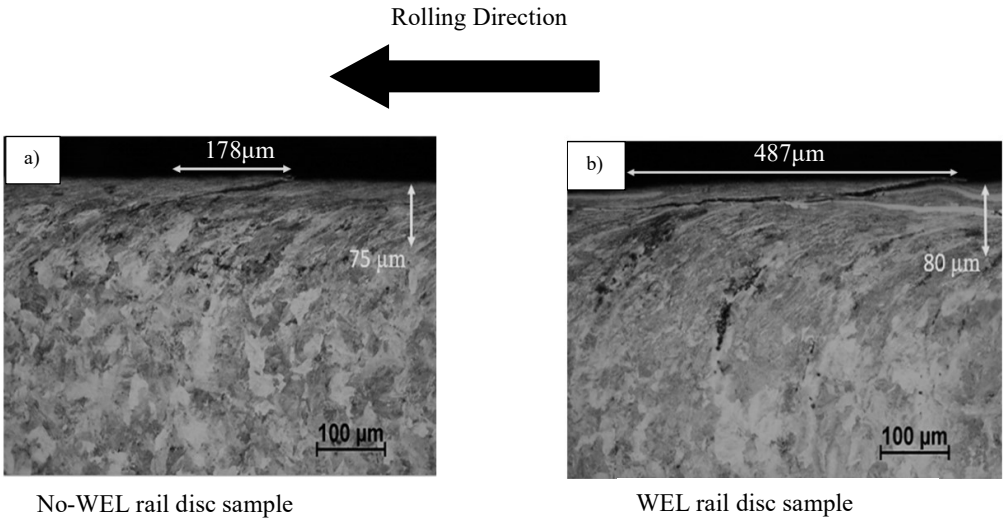

Figure 5-1: Rail disc sections in the rolling direction after 8000 cycles and 1% slip twin-disc testing for two cases a) A sample without WEL b) A sample with WEL [36]**.**

The mechanism presented in Figure 4-5 describes the deformation of WEL and its contribution to the crack initiation. The hypothesis was initially conceived by observing Figure 4-4. Further clarification of this mechanism can be done utilising samples acquired from the field. The samples were taken from a previous study of an R400 HT ground rail that underwent a number of cycles. Images in Figure 5-2 clearly exhibits the deformation of WEL where the asperities formed by grinding are smoothed out due to the run-in process. Furthermore, Figure 5-2a clearly shows the formation of crack on the WEL due to the rolling/sliding process and some asperities being crushed and ready to be detached. Figure 5-2b exhibits a substantial crack that was potentially produced due to the WEL. Moreover, near the cracks detected, the primary stages of the overlay effect take place where the pearlite is plastically deformed and gradually overlaying the remainings of the WEL.

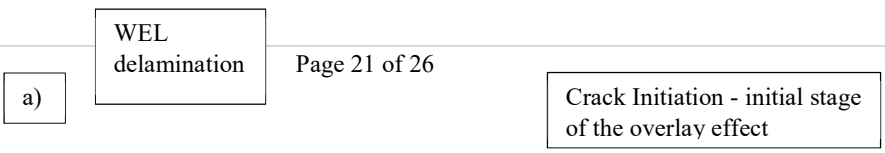

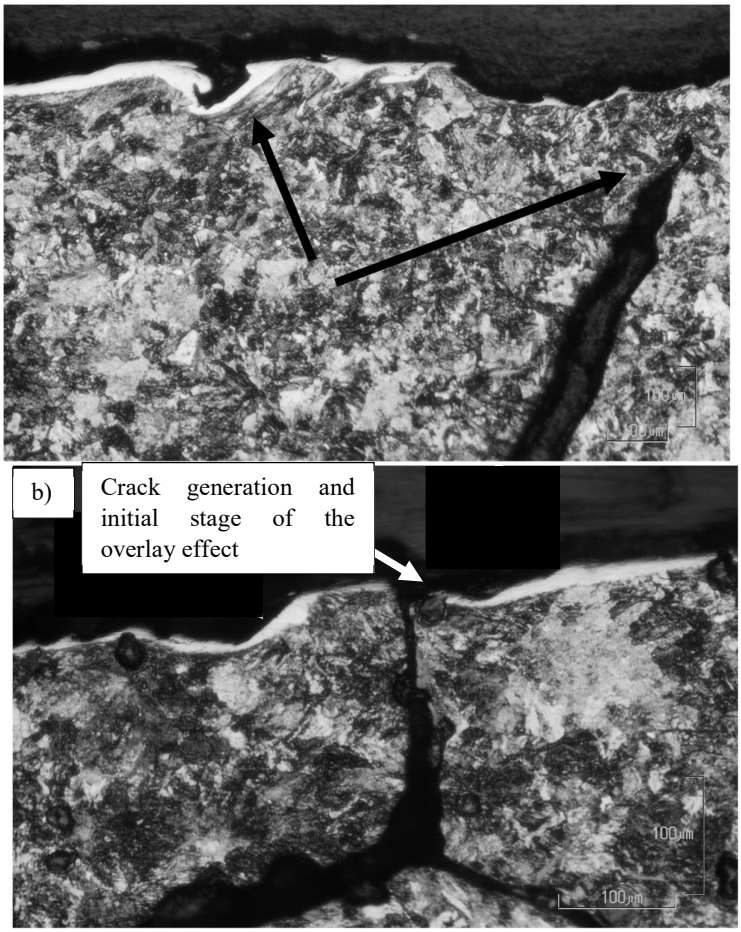

Figure 5-2: Post-grinding deformation of WEL.

In the hardness analysis that was done on the laboratory and field sample three main key facts were revealed. The existence of WEL from the significantly higher top layer hardness value compared to the bulk material hardness value, indicating the brittle nature of the layer. The second point is the relatively similar nano-hardness values of WEL. Considering the inhomogeneity of each pearlitic microstructure and the variation of the results due to individual grain orientation it can be said that the hardness of the WEL observed in the two samples is comparable. Finally, a transition region between WEL and bulk material was identified from the nano-hardness data in Figure 4-8 and SEM images in Figure 4-1. Moreover the transition region between the laboratory specimen and the field specimen differs as shown from the SEM images (Figure 4-1and Figure 4-2) and from nano-hardness tests (Figure 4-8 and Figure 4-9) indicating the different amounts of energy involved in each case. However, it is unclear the transition-region in the field sample was generated due to the grinding process or pre-existed. Nevertheless, further tests need to be done to examine the effect of the grinding induced transition region to the crack formation.

In the second part of this study the interaction between two bodies, the ground rail disc and the fresh surface wheel disc was observed. In this tribo-system friction alternates during their interaction based on the surface and material properties. The transitions the discs undergo, occur in an attempt for the tribo-system to reach a steady state condition [37]. Observing Figure 4-11c it can be said that after the run-in process the ground surface is possibly experiencing a decrease in roughness leading to a drop on the friction force as asperities become smoother and surfaces slide more freely. This is then followed by the steady state region where roughness and friction remain relatively stable. After a number of cycles the two surfaces start to experience severe wear leading to a slight increase in the frictional forces of the system as well as the surface roughness of the discs [38]. Similar behaviour has been presented by Blau et al. [37][39][40] on previous studies as one of the common behaviours which can be observed in sliding surfaces. As it can be seen in Figure 5-3 the studies support that specific tribo-systems

experience similar transitions with the three main regions presented as run-in, mild wear/steady-state, and severe wear. The development of roughness is further observed in Figure 4-14 where the profile of the rail disc was examined on 4 important points, 0 cycles, 1800 cycles, 3600 cycles and 8000 cycles. The data acquired is in agreement with pattern described in Figure 5-3b by Blau [37] where the roughness starting point is relatively high as a consequence of the grinding process. Subsequently the surface becomes smoother until further wear starts, and wear debris appears on the surface increasing the roughness again.

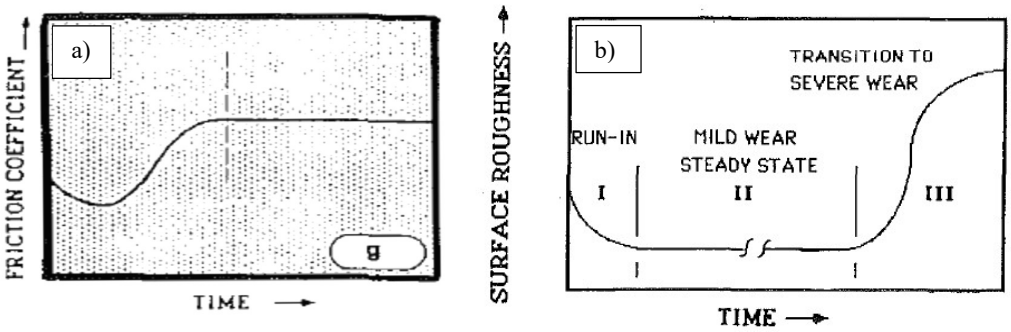

Figure 5-3: a) Presented by Blau [39] **as one of the commonly observed behavior in friciton coeffcient against time studies; b) Visual representation of the roughness transition from break-in period to steady state and wear region** [37]**.**

Compared to the results obtained and presented in Figure 4-11 the development of the coefficient of friction on regular fresh machined surface discs at a rolling contact testing with 1% slip is presented in Figure 5-4. The data presented are from a study performed by Santa et al. to assess the wear regime transitions in dry and wet cycles [41]. The experiments were done with a slip ratio of 1% and a maximum contact pressure of 1300MPa. The response from first 8000 dry cycles can be used for comparison with the data presented in this study. The run-in period of the discs lasts for approximately 1000 cycles where the coefficient of friction starts from a very low value and increases up to its maximum value. It will then settle on a lower value and remain stable for the rest of the test until significant wear occurs. This demonstrates the difference on the coefficient of friction when surfaces' roughness varies. Hence controlling the post-grinding roughness is crucial since it can substantially affect the friction between rail and wheel.

Moreover, from Figure 4-11b, it is clear that the controller on the SUROS machine responds relatively slowly to a difference between measured and requested slip; it can take 80 cycles to achieve 1% slip after the machine has been stopped to take replicas of the surfaces. It was important to wait for the correct slip before recording friction coefficient values.

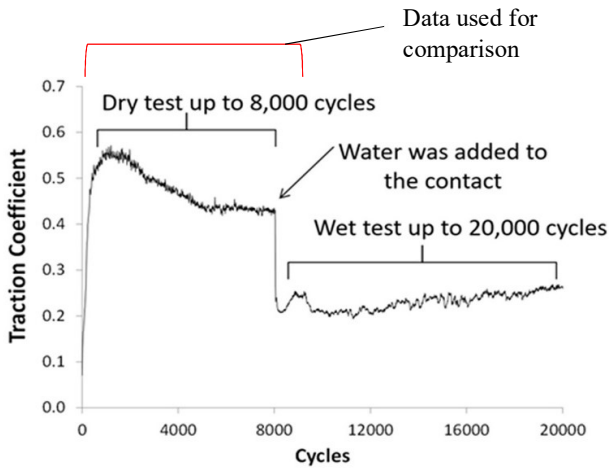

Figure 5-4: Typical performance of the coefficient of friction under dry and wet conditions for 1% slip and a maximum contact pressure of 1300MPa [41]**.**

A comparison of the wear rate obtained by the experiments and previous studies [28] done using fresh surface discs from R260 material exhibits a significant difference in the mass loss. It was observed by Santa et al. that the R260 disc under dry tests up to 8000 cycles exhibits a wear rate of 6.9µg/cycle compared to the total wear rate of 3.57 µg/cycle from the current experiment. The difference in wear rate indicates that the WEL on top of the disc surface might be acting as a protective layer during the initial run-in and steady-state period. However, further experiments need to take place to distinguish whether WEL is not affecting the disc performance by initiating more cracks. Another factor that can be examined is the uniformity of WEL and its effect on crack propagation. Pre-existing cracks and discontinuities within the WEL could potentially be a source of weakness in the microstructure leading to the propagation of these defects into the pearlite.

As seen in Figure 4-11a, the 1% slip test developed a friction coefficient of 0.25 after about 650 cycles, although this value varied for the rest of the test as well as the roughness. A clear trend of increasing friction coefficient with decreasing roughness can be seen up to these values, but later points show no obvious correlation as shown in Figure 4-13. Moreover, Figure 4-11a shows that the 1% slip test exhibits a peak in friction coefficient of 0.35 before a thousand cycles, then reaches a steady value of about 0.17 and eventually rises again to 0.4. The roughness at that point decreases so that each disc in each direction has approximately the same roughness (Figure 4-12). It can be concluded that the friction coefficient cannot be predicted from the wheel or rail roughness, so measuring the roughness of wheels and rails after a derailment will not provide an indication of which value of friction is appropriate to use in dynamic analyses of the incident.

6 Conclusions

A laboratory demonstration of rail grinding was successfully performed on a rail disc specimen and the post grinding performance of the disc was studied. The results of the experiments can be summarised in the followings:

1. A laboratory grinding process was performed and parameters used in the field were simulated successfully. Effects such as WEL were detected on the microstructure of the ground discs, similar to field ground rail.
2. Twin-disc tests were undertaken to investigate if a value of friction could be predicted from the initial roughness of the discs. No useful correlation was found. The lowest coefficient of friction was associated with the roughest discs, but after a short distance the friction coefficient increased, and the discs became smoother.
3. The wear tests exhibited that WEL does not increase the wear of the disc. On the contrary the twin disc testing showed that WEL acted protectively for the first 2500 cycles. However, it contributed afterwards to the development of cracks.

Acknowledgements

The authors are grateful to the Royal Academy of Engineering for financial support through the Industry Academia Partnership Programme, project n. IAPP\1516\91, and to the Metro de Medellín for providing rails and wheels for study.

References

[1] Z. Li, R. Dollevoet, M. Molodova, and X. Zhao, "Squat growth—Some observations and the validation of numerical predictions," *Wear*, vol. 271, no. 1–2, pp. 148–157, May 2011.

[2] V. Reddy, G. Chattopadhyay, P.-O. Larsson-Kraik, and T. Allahmanli, "Evaluation of technical vs economic decisions in rail grinding," in *2008 IEEE International Conference on Industrial Engineering and Engineering Management*, 2008, pp. 496–500.

[3] Wongm, "Four grinding wheels on this side, adjustable angles - Wongm's Rail Gallery." [Online]. Available: https://railgallery.wongm.com/track-machines/rail-grinder-rr24m30/E100_8612.jpg.html. [Accessed: 15-Apr-2019].

[4] R. Singleton, A. Bell, M. Marshall, and R. Lewis, "New Techniques for Faster Rail Grinding For Network Rail," Sheffield, 2011, Internal report, unpublished.

[5] R. Singleton, M. B. Marshall, R. Lewis, and G. Evans, "Rail grinding for the 21st century - Taking a lead from the aerospace industry," *Proceedings of the Institution of Mechanical Engineers, Part F: Journal of Rail and Rapid Transit*, vol. 229, no. 5. pp. 457–465, 2015.

[6] Z. Y. Zhang *et al.*, "Thermal model and temperature field in rail grinding process based on a moving heat source," *Appl. Therm. Eng.*, vol. 106, pp. 855–864, 2016.

[7] J. E. Stead, "Micro-metallography and its practical applications," *J. West Scotl. Iron Steel Inst.* , vol. 19, pp. 169–204, 1912.

[8] Y. Zhou, J. F. Peng, Z. P. Luo, B. B. Cao, X. S. Jin, and M. H. Zhu, "Phase and microstructural evolution in white etching layer of a pearlitic steel during rolling–sliding friction," *Wear*, vol. 362–363, pp. 8–17, Sep. 2016.

[9] "Locomotive derailment at Ordsall Lane Junction, Salford, 23 January 2013," 2014.

[10] H. Wu, X. Shu, and N. Wilson, *TCRP Report 71: Volume 5: Flange Climb Derailment Criteria and Wheel/Rail Profile Management and Maintenance Guidelines for Transit Operations*. Transportation Research Board, 2005.

[11] P. Allen and A. Bevan, "Determination of Tramway Wheel and Rail Profiles to Minimise Derailment," 2008.

[12] Pocock J., "Derailment mitigation - Categorisation of past derailments (T078)," *London Rail Saf. Stand. Board*, 2003.

[13] M. J. Nadal, "Théorie de la stabilité des locomotives, Part 2: Mouvement de Lacet," *Ann. des Mines*, vol. 10, pp. 232–366, 1896.

[14] J. Santamaria, E. G. Vadillo, and J. Gomez, "Influence of creep forces on the risk of derailment of railway vehicles," *Veh. Syst. Dyn.*, vol. 47, no. 6, pp. 721–752, 2009.

[15] J. Zeng and Q. H. Guan, "Study on flange climb derailment criteria of a railway wheelset," *Veh. Syst. Dyn.*, vol. 46, no. 3, pp. 239–251, 2008.

[16] K. L. Johnson, *Contact mechanics*. Cambridge University Press, 1987.

[17] E. A. H. Vollebregt, "Numerical modeling of measured railway creep versus creep-force curves with contact," *Wear*, vol. 314, no. 1, pp. 87–95, 2014.

[18] S. Fukagai, H. P. Brunskill, A. K. Hunter, R. S. Dwyer-Joyce, and R. Lewis, "Transitions in rolling-sliding wheel/rail contact condition during running-in," *Tribol. Int.*, vol. online 17, 2019.

[19] C. J. Rasmussen, S. Fæster, S. Dhar, J. V. Quaade, M. Bini, and H. K. Danielsen, "Surface crack formation on rails at grinding induced martensite white etching layers," *Wear*, vol. 384–385, no. March, pp. 8–14, 2017.

[20] D. Zapata, J. F. Santa, J. C. Sánchez, J. C. González, and A. Toro, "Effect of rail grinding conditions on sub-surface microstructure and surface roughness of fatigued rails," *Proc. - Int. Brazilian Conf. Tribol.*, 2010.

[21] B. Lin, K. Zhou, J. Guo, Q. Y. Liu, and W. J. Wang, "Influence of grinding parameters on surface temperature and burn behaviors of grinding rail," *Tribol. Int.*, vol. 122, pp. 151–162, Jun. 2018.

[22] M. H. Zhu, Z. R. Zhou, and J. J. Liu, "Current state of the research of tribological white layer," *Tribol. Mater. surfaces interfaces*, vol. 19, no. 3, p. 281, 1999.

[23] E. Uhlmann, P. Lypovka, L. Hochschild, and N. Schröer, "Influence of rail grinding process parameters on rail surface roughness and surface layer hardness," *Wear*, vol. 366–367, pp. 287–293, 2016.

[24] S. Fukagai, L. Ma, and R. Lewis, "Tribological aspects to optimize traction coefficient during running-in period using surface texture," *Wear*, vol. 424–425, pp. 223–232, 2019.

[25] H. Doi, T. Miyamoto, J. Suzumura, J. Nakahashi, H. Chen, and T. Ban, "Change in Surface Condition of Turned Wheel and Effectiveness of Lubrication against Flange Climb Derailment," *Q. Rep. RTRI*, vol. 53, no. 2, pp. 70–76, 2012.

[26] J. Lundmark, E. Kassfeldt, J. Hardell, and B. Prakash, "The influence of initial surface topography on tribological performance of the wheel/rail interface during rolling/sliding conditions," *Proc. Inst. Mech. Eng. Part F-journal Rail Rapid Transit*, vol. 223, no. 2, pp. 181–187, 2009.

[27] D. Yamamoto and H. Chen, "A Fundamental Study on Fine Unevenness and Tangent Force on Wheel Tread of Railway Vehicle (Relations between Environmental Condition and Tangent Force Characteristics with a Two-Disk Rolling Machine)," *Trans. JAPAN Soc. Mech. Eng. Ser. C*, vol. 77, no. 781, pp. 3211–3222, 2011.

[28] J. F. Santa *et al.*, "Twin disc assessment of wear regime transitions and rolling contact fatigue in R400HT – E8 pairs," *Wear*, vol. 432–433, p. 102916, Aug. 2019.

[29] R. Lewis, P. Christoforou, W. J. Wang, A. Beagles, M. Burstow, and S. R. Lewis, "Investigation of the influence of rail hardness on the wear of rail and wheel materials under dry conditions (ICRI wear mapping project)," *Wear*, vol. 430–431, pp. 383–392, Jul. 2019.

[30] D. Petersen, R. Link, D. Fletcher, and J. Beynon, "Development of a Machine for Closely Controlled Rolling Contact Fatigue and Wear Testing," *J. Test. Eval.*, vol. 28, no. 4, p. 267, 2000.

[31] R. Lewis, R. S. Dwyer-Joyce, and J. Lewis, "Disc machine study of contact isolation during railway track sanding," *Proc. Inst. Mech. Eng. Part F J. Rail Rapid Transit*, vol. 217, no. 1, pp. 11–24, Jan. 2003.

[32] K. Zhou *et al.*, "Experimental investigation on material removal mechanism during rail grinding at different forward speeds," *Tribol. Int.*, vol. 143, p. 106040, Mar. 2020.

[33] P. A. Cuervo, J. F. Santa, and A. Toro, "Correlations between wear mechanisms and rail grinding operations in a commercial railroad," *Tribol. Int.*, vol. 82, no. PB, pp. 265–273, Feb. 2015.

[34] J. F. Santa, A. Toro, and R. Lewis, "Correlations between rail wear rates and operating conditions in a commercial railroad," *Tribiology Int.*, vol. 95, pp. 5–12, 2016.

[35] M. Steenbergen, "Rolling contact fatigue in relation to rail grinding," *Wear*, vol. 356–357, pp. 110–121, 2016.

[36] B. Lopez, "Effect of White Etching Layer on the rolling contact fatigue behavior - October 2019 update," Medellin, Colombia, 2019.

[37] P. J. Blau, "A Model for Run-In and Other Transitions in Sliding Friction," *J. Tribol.*, vol. 109, no. 3, p. 537, 2009.

[38] P. J. Blau, "On the nature of running-in," *Tribol. Int.*, vol. 38, no. 11–12, pp. 1007–1012, Nov. 2005.

[39] P. J. Blau, "Interpretations of the Friction and Wear Break-in Behavior in Metals in Sliding Contact.," *Wear*, vol. 71, no. 1, pp. 29–43, 1981.

[40] P. J. Blau, "On the nature of running-in," *Tribol. Int.*, vol. 38, no. 11–12, pp. 1007–1012, Nov. 2005.

[41] J. F. Santa *et al.*, "Twin disc assessment of wear regime transitions and rolling contact fatigue in R400HT – E8 pairs," *Wear*, 2019.